IEEE Access
Multidisciplinary | Rapid Review | Open Access Journal

Received September 4, 2018, accepted October 15, 2018, date of publication October 29, 2018,
date of current version November 30, 2018.

Digital Object Identifier 10.1109/ACCESS.2018.2878267

Comparative Study of Three Different Radial Flux Ironless BLDC Motors

LIU YANG[1], JING ZHAO[1], (Member, IEEE), XIANGDONG LIU[1], (Member, IEEE), A. HADDAD[2], (Member, IEEE), JUN LIANG[2], (Senior Member, IEEE), AND HENGZAI HU[3]

[1]School of Automation, Beijing Institute of Technology, Beijing 100081, China
[2]School of Engineering, Cardiff University, Cardiff CF24 3AA, U.K.
[3]Department of Power Supply, Beijing Machine and Equipment Institute, Beijing 100854, China

Corresponding author: Jing Zhao (zhaojing_bit@bit.edu.cn)

This work was supported in part by the National Natural Science Foundation of China under Project 51677005, in part by the Major Project of Zhongshan City under Grant 2016A1027, and in part by the Key Laboratory for Intelligent Control and Decision of Complex Systems, Beijing Institute of Technology.

ABSTRACT Three different radial flux ironless brushless dc (BLdc) motor types (motors without inner back-iron of the rotor, with inner back-iron of the rotor, and with dual-rotor) are investigated and compared in this paper. The magnetic field distribution, back electromagnetic force (EMF), axial end effect, and torque characteristics are investigated. First, the relationship between the magnetic field distribution and the motor size and pole pairs is investigated. It shows that the two parameters are not independent of each other and the magnetic field distribution is mainly related with the arc length of the permanent magnets. Second, the radial magnetic flux density in the coil regions of the three ironless BLdc motors is calculated and an evaluation factor is proposed to show the quality of the magnetic field distribution. Third, the influence of the winding configuration and the combination of slot and pole number on EMF is analyzed, and the corresponding evaluation factors are calculated and tabulated. Then, the axial end effect of the three ironless BLdc motors considering the fringe effect is investigated and compared. Next, the torque characteristics at full load and rated speed are studied for the three types of motors. Finally, the ironless BLdc motor without back-iron of the rotor is manufactured and tested. The experimental results are in good agreement with the finite-element method.

INDEX TERMS Ironless BLDC motor, magnetic field, axial end effect, back EMF, torque characteristics.

I. INTRODUCTION

Due to high efficiency, compactness, long life, small volume and high power/weight ratio, the brushless dc (BLDC) motors have become the obvious and most popular choice for industrial applications [1]–[7]. Compared to ordinary BLDC motors, the stator of an ironless BLDC motor is made not of iron but of a nonmagnetic plastic material, which makes the flux linkage harmonics caused by iron stator slots and magnetic saturation absent, and the cogging and reluctance torque ripples greatly reduced [8]–[12]. Three main ironless BLDC motor topologies, which are motors without inner back-iron of the rotor [8], [10], [12], with inner back-iron of the rotor [13] and with dual-rotor [4], [14], as shown in Fig. 1, have received widespread acceptance in various industrial applications. Fig. 1 (a) to (c) illustrate the above mentioned three different ironless BLDC motor topologies with Type I, Type II and Type III, respectively. As shown in Fig. 1, the stator parts of the three ironless BLDC motors mainly include the phase windings, and the nonmagnetic stator frame which is not showing and can be instead by air. For Type I, the rotor parts include the outer PMs and the outer back-iron. For Type II, the rotor parts include the outer PMs, outer and inner back-irons. And for Type III, the rotor parts include the outer and inner PMs, the outer and inner back-irons. Furthermore, as for Type I, the outer rotor of the motor is made of a thin cup-shaped cylindrical steel drum, the permanent magnets (PMs) are mounted on the inner surface of the outer rotor's back-iron. And for Types II and III, the rotor core consists of outer and inner back-irons, the outer PMs are mounted on the inner surface of the outer back-irons of Types II and III, and the inner PMs are mounted only on the outer surface of the rotors' inner back-iron of Type III.

Some researchers have done some studies on each of the presented three ironless BLDC motor types. In [8], the

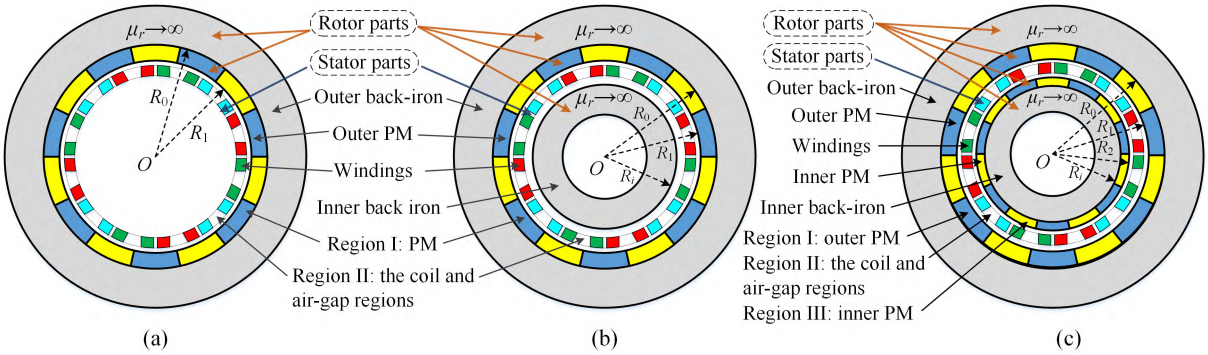

FIGURE 1. The models of the three different ironless BLDC motor types (14P12S). (a) Type I. (b) Type II. (c) Type III.

magnetic field of the motor, which adopted an ''inside-out'' construction with an internal ironless stator (i.e. Type I in this paper), is analyzed with the end effects neglected. However, as a result of the inside-out design, this type motors invariably have a high number of pole pairs and high rotor inertia. In [10], the machine with an outer-rotor and a coreless stator (i.e. Type I in this paper) is investigated to suit applications in clean energy generation and storage systems. Correspondingly, its rotational torque and back EMF are computed to meet the maximum torque. In [13], an ironless BLDC motor with an inner back-iron on the rotor and with PMs mounted only on the corresponding outer back-iron (i.e. Type II in this paper) is studied to achieve a high efficiency. The air gap magnetic field distribution and back EMF were investigated by FEM, and the impedances of the end part are taken into account in the circulating current losses calculation. Studies have been found that Halbach array PM machines can provide unilateral magnetic flux and obtain high magnetic flux density in the air gap [15], [17]. Hence, as for the ironless PM machines, the Halbach array PMs are widely used to obtain a high and smooth torque and high efficiency [18], [20]. An ironless BLDC motor with enclosed-rotor and Halbach-array PMs mounted on both the outer and inner beck-irons of the rotor (i.e. Type III in this paper) is investigated [4], and the air gap flux density along the radius is studied without taking the axial end effect into consideration. In [14], a kind of ironless dual-rotor, radial-flux PM machine (similar to Type III) is proposed, and the end-winding effects to motors is just simply described. Also, the outer and inner portion of the rotor core are connected together by an end disc, which can work as a cooling fan. So, this class of machines (Type III) is found to be suitable for moderately high, even higher speed critical space applications, which warrants the utmost accuracy and least value of cogging torque, due to its high torque density, high efficiency and the ironless stator. However, to the authors' knowledge, no published paper has compared the electromagnetic characteristics of the presented three ironless BLDC motors with the same volume and similar configurations.

All the above papers have proven the ironless BLDC motors can provide the best all-around performance for aerospace and industrial applications. For different applications and performance requirements, the structures of the BLDC motors are different. However, almost all published papers focused only on one kind of motor. In general, the stator parts of the ironless BLDC motors are similar, e.g. the same concentrated windings and non-magnetic stator frame. Hence, the main structural difference lies in the rotor part. In view of the rotors' structural differences of the presented three ironless BLDC motor types, the magnetic field distribution, electromagnetic force (EMF), axial end effect and torque characteristics will be different for each type. Moreover, considering the stators of the presented three different ironless BLDC motor types made of nonmagnetic materials, there is no stator iron to guide magnetic flux paths. Then, the ironless BLDC motors will suffer from a general lower magnetic flux crossing the air gap, which will result in a lower power output in the stator's ironless design compared to the equivalent stator iron design. In order to distinguish the electromagnetic properties and provide some selection bases, the electromagnetic characteristics of the presented three different ironless BLDC motor types are studied and compared in this paper.

In this paper, the magnetic field distribution of the presented three different ironless BLDC motors is achieved firstly. The waveform quality of the radial magnetic flux density with the motor size and pole pairs is evaluated and compared. Meanwhile, an evaluation factor is introduced to evaluate the radial component of the flux density. Secondly, the proposed evaluation factors of the back EMFs of the three motor types are calculated, with the consideration of the winding configurations of overlapping and non-overlapping types. Thirdly, the axial end effect with different axial lengths of the presented three motors is investigated by the introduced correction factor. Fourthly, the torque characteristics at full load and rated rotational speed are investigated and compared. Finally, a prototype of the ironless BLDC motor without the inner back-iron of the rotor (i.e. Type I in this

paper) is designed, manufactured and tested to validate the simulation results.

II. COMPARISON OF THE MAGNETIC FIELD CHARACTERISTICS

The magnetic field distribution of the ironless BLDC motors is not only related to the pole pairs, but also to the motor size (viz. the outer PMs' inner diameter of the rotor). However, the pole pairs and the motor size are not completely independent of each other. In order to reduce the number of the variables, the arc-length of the PM L_{PM} is introduced, which is defined as

$$L_{PM} = \frac{2\pi R_1}{p} \tag{1}$$

where R_1 is the inner radius of the outer PM, which can represent the motor size, and p is the pole pairs.

In order to compare the electromagnetic properties of the three ironless BLDC motors under the same PM magnetization, the magnetization types of the PMs are of parallel in this paper, which is easy to impose both in FEM simulation and in real machine manufacturing process. Other magnetizations, such as radial, sinusoidal, Halbach array, etc., can be studied in the same way, which are not included in this paper.

The magnetic flux lines distribution of the three ironless BLDC motor types with the same R_1 of 25mm, are illustrated in Fig. 2. As it can be seen, the distribution of the magnetic flux lines in the air gap of Type III is more uniform and denser than that of the other two types. In addition, the amplitude of the magnetic field of Type III is about 6% and 8% higher than that of Type II and Type I, respectively.

As for the models of the presented three different ironless BLDC motor types shown in Fig. 1, the magnetic characteristics (i.e. the radial and tangential magnetic flux densities) of each motor type are compared with different motor sizes. In order to investigate and synthetically compare the magnetic field distribution in the coil regions of the presented three motor types, the arc-lengths of the outer PMs maintain constant through changing the proportionally both number of pole pairs p and the inner radius of the outer PMs R_1. The main parameters of the presented three motor types with the same L_{PM} are listed in Table 1.

TABLE 1. Parameters of the presented three ironless BLDC motor types.

Parameter	Type I	Type II	Type III
Inner radius of outer PM, R_1	25/50/75/100 mm		
Pole pairs, p	2/4/6/8		
Outer radius of outer PM, R_o	R_1+4mm		
Outer radius of inner PM, R_2	-	-	R_1-5mm
Outer radius of Back-iron, R_i	-	R_1-5mm	R_2-3mm
Relative permeability of the PMs, μ_r	1.043		
Residual flux density of the PMs, B_r	1.28T		
Effective axial length of the motor, L_{ef}	12mm		

The corresponding waveforms of the radial magnetic flux density $B_{r\mathrm{II}}$ and the tangential magnetic flux density $B_{\theta\mathrm{II}}$ in Region II (i.e. the coil and air-gap regions as shown in Fig. 1)

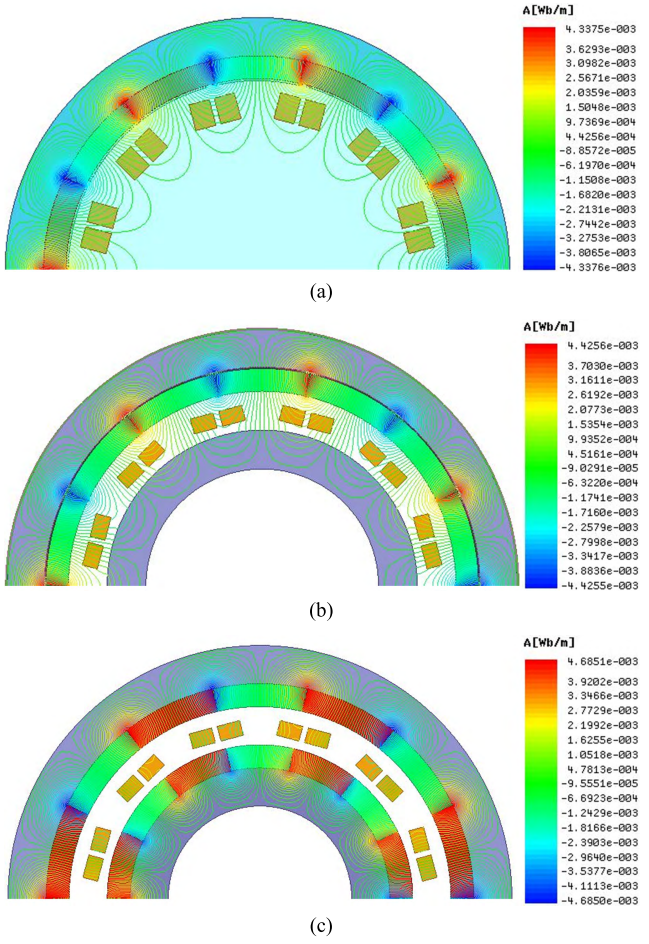

FIGURE 2. Magnetic flux lines distribution of the three ironless BLDC motor types with R_1 = 25mm. (a) Type I. (b) Type II. (c) Type III.

of the presented three ironless BLDC motor types are shown in Fig. 3. The calculated positions of the magnetic flux density of the three motor types are $r = (R_1 - 1)$ mm. It can be seen that the magnetic flux densities of each of the ironless BLDC motor types are identical with the same L_{PM}. The small discrepancy may be attributed to the influence of the motor curvature.

As is known, the radial magnetic flux density is closely related to the back EMF of radial flux motors. In order to show the space distribution of the radial magnetic flux density $B_{r\mathrm{II}}$ in Region II of the presented three motor types, the waveforms of the $B_{r\mathrm{II}}$ with different radii in the coil region for the three motor types with $p = 8$ and $R_1 = 60$mm are shown in Fig. 4. Δr means the radius difference of the calculation position r to the inner radius of external PMs R_1. It can be seen from the above results that the amplitude of the magnetic flux density of Type III is bigger than that of the other two types, and that Type I is the smallest. Besides, the radial magnetic flux density $B_{r\mathrm{II}}$ in the coil region of Type I changes greater than that of the other two types.

As the 120° commutation control is generally used for the BLDC motors, the ideal back EMF should be trapezoidal.

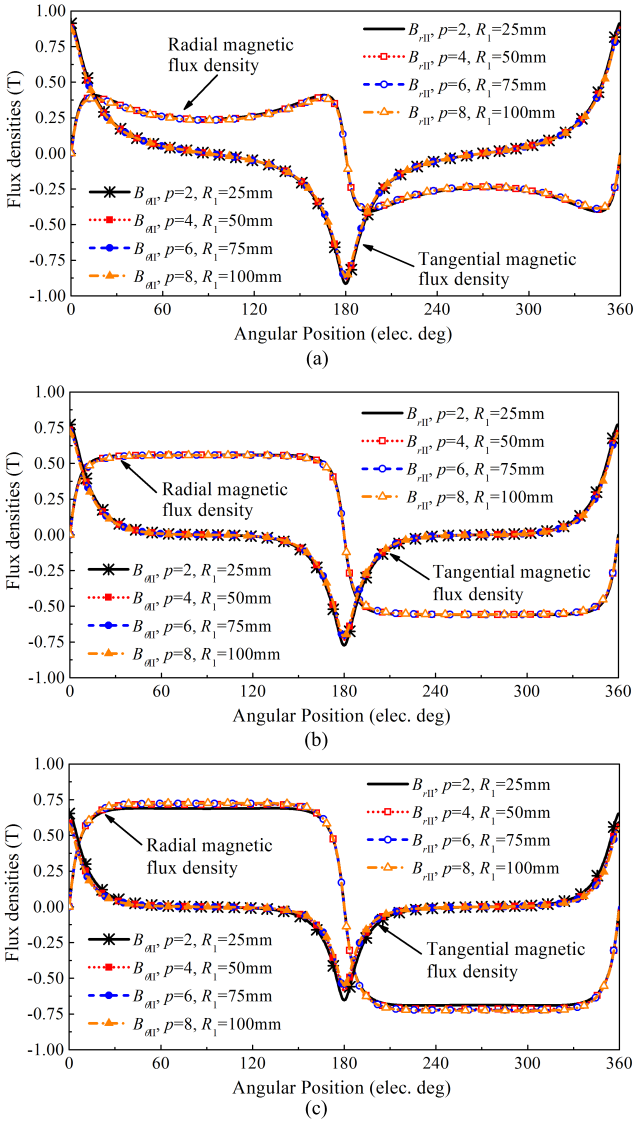

FIGURE 3. The magnetic flux density waveforms with the same L_{PM} of the presented three ironless BLDC motor types. (a) Type I. (b) Type II. (c) Type III.

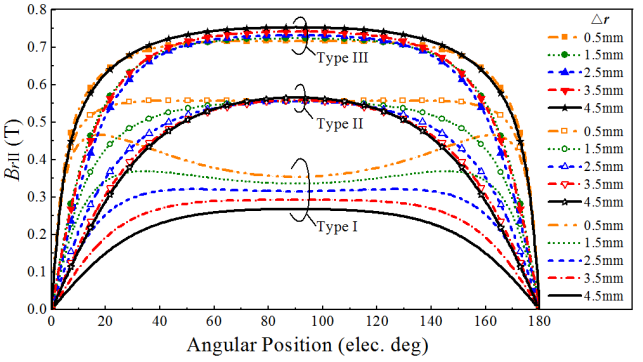

FIGURE 4. The waveforms of B_{rII} of the three different ironless BLDC motor types with $p = 8$ and $R_1 = 60$mm.

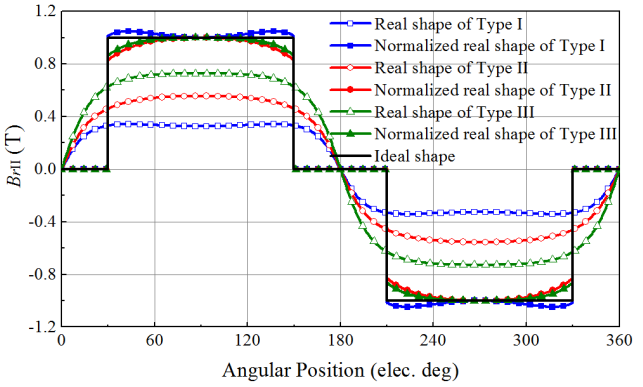

FIGURE 5. The normalized radial magnetic flux densities at $r = 59$mm during the 120° elec. deg. of the three different ironless BLDC motor types with $p = 8$ and $R_1 = 60$mm.

Furthermore, because the waveform of the back EMF mainly depends on the shape of $B_{r\mathrm{II}}$, the ideal shape of $B_{r\mathrm{II}}$ also should be trapezoidal with a flat-top width larger than 120° elec. deg. However, as it can be seen from Fig. 4, the shapes of the waveforms are not trapezoidal.

In Fig. 5, the waveforms of $B_{r\mathrm{II}}$ at $r = 59$mm of the studied three motor types with $p = 8$ and $R_1 = 60$mm are presented. Meanwhile, the waveforms during the 120° elec. deg. period are cut out and normalized considering the 120° commutation control. During the normalization process of $B_{r\mathrm{II}}$ of the three motor types, the values of $B_{r\mathrm{II}}$ at 90° elec. deg. ($B_{r\mathrm{II}}$-90° for short) of each the motor type are chosen as the base values, correspondingly. It can be seen from Fig. 5 that the fitting degree between the normalized real shape and the ideal shape of the $B_{r\mathrm{II}}$ of the presented three motor types are different. In order to better evaluate the quality of $B_{r\mathrm{II}}$, an evaluation factor ζ_e is proposed and this approach indicates that the smaller the value of ζ_e is, the better will be the shape of the trapezoidal waveform. The evaluation factor ζ_e is defined as

$$\zeta_e = \sqrt{\sum_{n=1,2,3,\ldots}^{\infty} (\alpha_n - \beta_n)^2} \tag{2}$$

where α_n is the nth harmonics of the normalized radial magnetic flux density, and β_n is the nth harmonics of the ideal waveform.

In order to compare the magnetic flux density and evaluate the quality of the waveforms, in this work, the pole pairs is set to 8 and the inner radius of the outer PMs R_1 is varying from 20mm to 100mm with the step size of 20mm. The amplitude of $B_{r\mathrm{II}}$-90° with different R_1 and the corresponding evaluation factor ζ_e of the three ironless BLDC motor types are shown in Fig. 6. From the amplitude comparison, it can be seen that: (i) corresponding to Fig. 4, the variations of the $B_{r\mathrm{II}}$-90° of Type I values are larger along with the motor size changing compared with those of the other two types, and this is attributed mainly to the lack of the inner back-iron of the rotor. (ii) with a certain R_1, $B_{r\mathrm{II}}$-90° of Type III is the largest, the next is Type II, and the smallest is Type I, which is consistent with Fig. 4. Moreover, Fig. 4 indicates

that the ironless BLDC motor with dual-rotor has the highest power density. (iii) for Type II and Type III, when R_1 is bigger than 40mm, the magnitude of $B_{r\mathrm{II}}$-90° along different radii for a certain R_1 shows negligible changes. This results in circulating current reduction when the windings are in parallel. In addition, from the comparison of ζ_e, it can be seen that: (i) for Type II and Type III, the ζ_e decreases with increasing motor size and for positions close to the PMs' surface. (ii) As for Type I, the ζ_e increases with the motor size when the position is close to the inner surface of the outer PMs. However, it decreases with increasing motor size when the position is far away from the inner surface of the outer PMs.

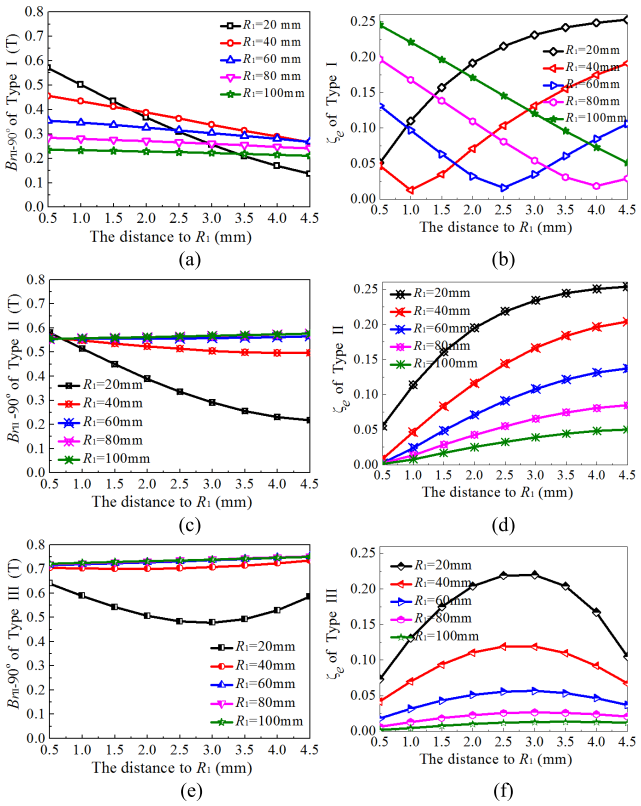

FIGURE 6. The $B_{r\mathrm{II}}$-90° and ζ_e of the presented three ironless BLDC motor types at different radii with $p = 8$. (a) $B_{r\mathrm{II}}$-90° of Type I. (b) ζ_e of Type I. (c) $B_{r\mathrm{II}}$-90° of Type II. (d) ζ_e of Type II. (e) $B_{r\mathrm{II}}$-90° of Type III. (f) ζ_e of Type III.

On one hand, it can be said conclusively that, with the same arc-length of the PMs of the three motor types, the magnitude of the radial magnetic flux density of Type III is bigger than Type II, and that Type I is the smallest. On the other hand, the radial magnetic flux density waveforms' trapezoidal degree of both Type II and Type III are bigger than Type I. However, when the number of pole pairs is fixed, the trapezoidal degree of the radial magnetic flux waveforms of the three motors are different with the variations of motor size and the distance to the PMs, as is clearly indicated in Fig. 6, with $p = 8$.

III. COMPARISON OF THE WINDING CONFIGURATIONS AND THE AXIAL END EFFECT ON BACK EMF

A. EFFECT OF WINDING CONFIGURATION ON BACK EMF

Windings are one of the important components of motor, the wire gauge (i.e. the wire diameter) and winding configurations (e.g. single/double layer windings, concentrated winding, over/non-overlapping windings, etc.) influence the motor performance greatly. For the non-overlapping windings, either all the teeth or only the alternate teeth carry the coils. While for the overlapping windings, the short-pitch winding will make the shape of the back EMF closer to a sine wave, so only the full-pitch winding (i.e. the winding pitch equals to the PMs' polar distance) is considered. Three different winding configurations, named Winding I, Winding II and Winding III, respectively, are shown in Fig. 7. Table 2 shows the winding parameters when $R_1 = 25$mm.

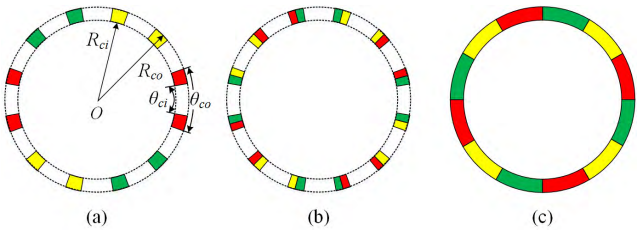

FIGURE 7. The three different winding configurations.
(a) Non-overlapping winding with alternate teeth wound (Winding I).
(b) Non-overlapping winding with all teeth wound (Winding II).
(c) Overlapping winding with full-pitch (Winding III).

TABLE 2. Parameters of the three different winding configurations.

Parameter	Winding I	Winding II	Winding III
Outer radius of coil region, R_{co}		24.5mm	
Inner radius of coil region, R_{ci}		20.5mm	
Slot pitch, θ_s		$2\pi/Q_s$	

Q_s is the number of virtual slots.

The magnetic linkage linked with a coil package ψ_{cp} can be expressed as

$$\psi_{cp} = \int_{R_{ci}}^{R_{co}} \int_{\theta_{ci}}^{\theta_{co}} \rho_c \left[L_1 \int_{-\theta_c/2}^{\theta_c/2} B_{r\mathrm{II}}(r,\theta)\, r d\theta \right] r d\theta_c dr \quad (3)$$

where ρ_c is coil density; dr, $d\theta_c$ are the differentiation elements of the coil package's radius and angle, respectively.

The back EMF depends on the distribution of the magnetic flux density in the air-gap region and the winding type. So, the evaluation factor has to be applied on the back EMF. According to Faraday's law, the back EMF induced in each coil package e_{cp} can be obtained by

$$e_{cp} = -\frac{d\psi_{cp}}{dt} \quad (4)$$

Since the amplitude of the back EMF is dominated by the amplitude of $B_{r\mathrm{II}}$, only the evaluation factor of the back EMF

TABLE 3. ζ_e of the presented ironless BLDC motor of Type I.

Q_s \ $2p$	2	4	6	8	10	12	14	16	18	20	22	24	26	28
3	0.546	0.371												
6	0.563#	0.374		0.169										
9			0.321	0.114	0.062	0.053								
12		0.380#		0.337	0.189 0.061*		0.032 0.105*	0.033						
15					0.349		0.131	0.084		0.106				
18			0.253#			0.354	0.257	0.172		0.107	0.117	0.107		
21							0.356	0.273		0.160	0.137		0.145	0.129
24				0.160#				0.354		0.221 0.113*	0.183 0.142*		0.148 0.174*	0.142 0.186*

TABLE 4. ζ_e of the presented ironless BLDC motor of Type II.

Q_s \ $2p$	2	4	6	8	10	12	14	16	18	20	22	24	26	28
3	0.328	0.013												
6	0.005#	0.332		0.043										
9			0.339	0.174	0.092	0.078								
12		0.017#		0.344	0.216 0.098*		0.108 0.159*	0.108						
15					0.341		0.176	0.142		0.131				
18			0.033#			0.336	0.259	0.201		0.152	0.157	0.147		
21							0.332	0.269		0.189	0.171		0.172	0.160
24				0.050#				0.328		0.232 0.156*	0.204 0.174*		0.175 0.194*	0.169 0.199*

TABLE 5. ζ_e of the presented ironless BLDC motor of Type III.

Q_s \ $2p$	2	4	6	8	10	12	14	16	18	20	22	24	26	28
3	0.328	0.008												
6	0.003#	0.330		0.025										
9			0.333	0.165	0.070	0.049								
12		0.010#		0.338	0.210 0.078*		0.078 0.140*	0.075						
15					0.342		0.160	0.118		0.100				
18			0.020#			0.343	0.257	0.188		0.126	0.132	0.121		
21							0.341	0.270		0.173	0.150		0.153	0.137
24				0.031#				0.338		0.226 0.132*	0.191 0.155*		0.157 0.180*	0.149 0.186*

Values with superscript of * and # represent the ζ_e with Winding I and Winding III, respectively. Values without superscript represent the ζ_e with Winding II.

is analyzed. The evaluation factor ζ_e with different winding configurations and combinations of slot and pole numbers are calculated and listed in Tables 3 to 5. It can be observed from the tables that: (i) for Type II and Type III, the ζ_e of Winding III is smaller than that of both Winding I and Winding II, with the same pole pairs or with the same slot numbers for a certain motor of Type II or Type III. (ii) for each motor type, the ζ_e of Winding I is smaller than that of Winding II when the pole number is smaller than slot number, and vice versa. (iii) the ζ_e of Winding I increases with the increasing of the pole number for a certain slot number of each motor type. (iv) Type III has the smallest ζ_e for Winding II and Winding III when the pole number is smaller than 6. While for Winding II, Type I has the smallest ζ_e, when the pole number is larger than 20.

B. EFFECT OF THE AXIAL END ON THE BACK EMF

Considering the fringe effect of the PMs in ironless BLDC motors, the axial end effect cannot be ignored [21], [23]. In order to evaluate the axial end effect and account for the influence of the end windings on the back EMF, a correction factor *Ke* is introduced by carrying out a 3-D static FEM. The calculation factor *Ke* is defined as [12]

$$K_e\left(r, L_{ef}\right) = \frac{\int_0^{L_{ef}} B_{r\mathrm{II}3-\mathrm{D}}\left(r, \theta, z\right)}{B_{r\mathrm{II}2-\mathrm{D}}\left(r, \theta\right) \cdot L_1} \times 100\% \tag{5}$$

where $B_{r\mathrm{II}2-\mathrm{D}}(r, \theta)$ is the radial component obtained by the 2-D FEM calculation and $B_{r\mathrm{II}3-\mathrm{D}}(r, \theta, z)$ is obtained by the 3-D static FEM method. L_{ef} and L_1 are defined as the effective and actual axial lengths of the motor, respectively. Owing to the effective axial length L_{ef} is different for

different motor types, K_e is determined under the assumption that $L_{ef} = L_1$.

Considering the motor of Type I with the pole pairs of 7 had been manufactured, and the other dimension parameters are the same with the models investigated in this paper. Hence, in order to make full use of the existing experimental equipment in the laboratory. In the following results, the pole pair number of the three ironless BLDC motor types is set to 7, an R_1 is set to 25mm.

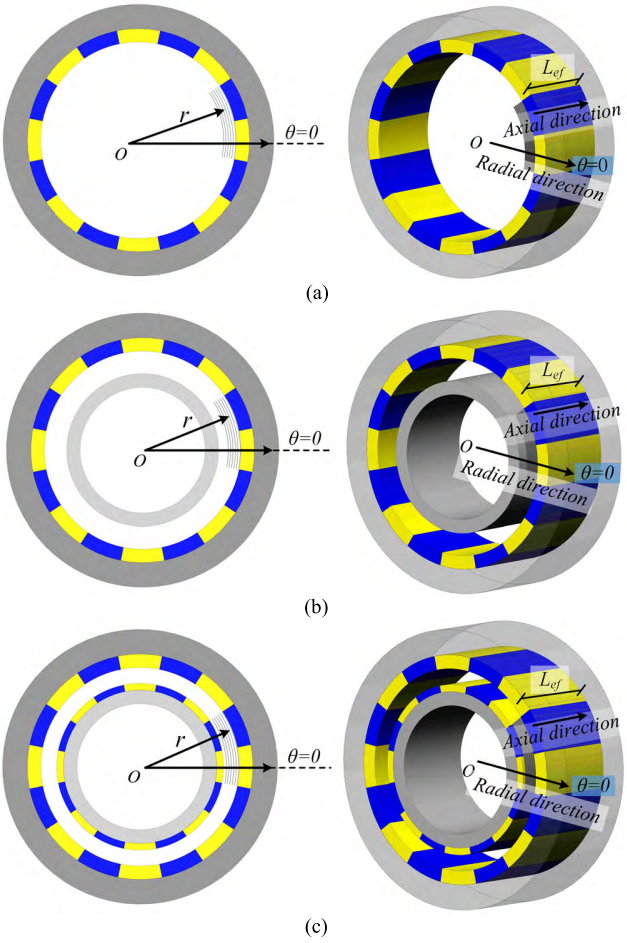

FIGURE 8. The 2-D and 3-D models of the three ironless BLDC motor types. (a) Type I. (b) Type II. (c) Type III.

The three different ironless BLDC motor types containing both 2-D and 3-D models are shown in Fig. 8. In order to simplify the analytical models in the magnetostatic simulation, the established models include only PMs (the pole-arc to pole-pitch ratio equals to 1) and the back-irons. Moreover, $\theta = 0$ (as it shows in Fig. 8) is selected as the position for the estimation of the parameter K_e.

The radial component of the flux density at position $r =$ 22.5mm in the middle of the coil region with $L_1 =$ 12mm, 30mm and 60mm of the three ironless BLDC motor types are shown in Fig. 9. The results include both 3-D and 2-D FEM results. It can be seen that, with the PMs distributed on both sides of the outer and inner back-irons of Type III, the magnetic flux density in Type III is about 50% higher than that of Type II. This indicates that there is more magnetic flux passing through the coil region in Type III. In addition, the waveforms of the radial magnetic flux density of the three ironless BLDC motor types show good agreement between the 2-D and 3-D FEM results along the axial length L_1.

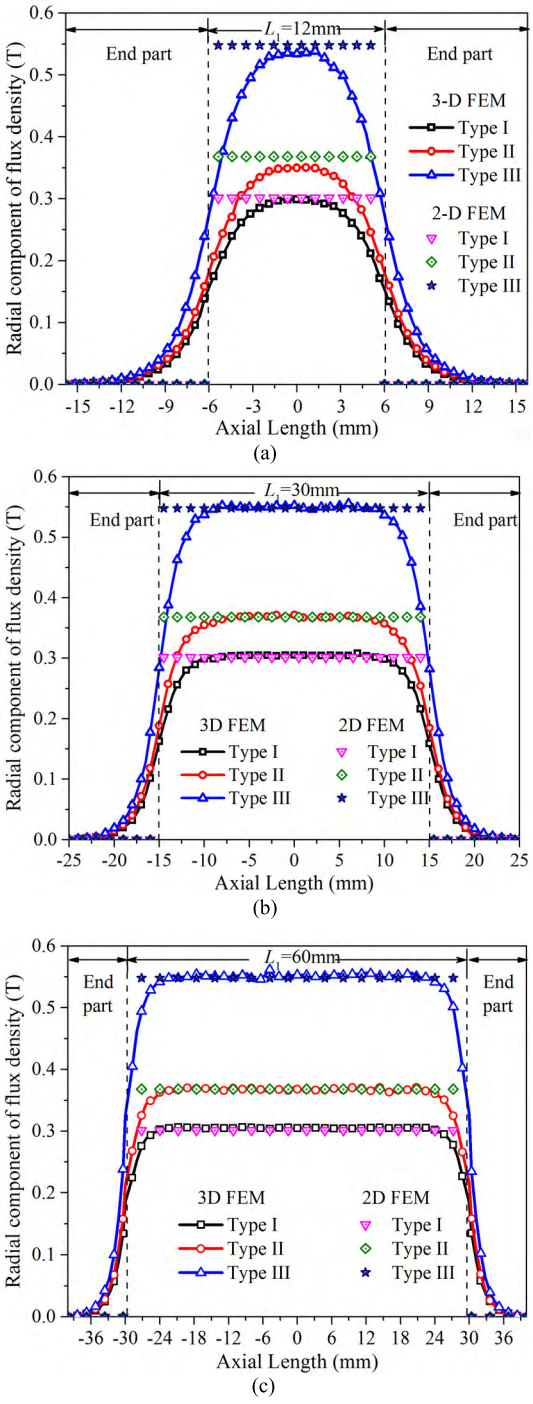

FIGURE 9. Radial component of flux density of the three different ironless BLDC motor types at $r = 22.5$mm. (a) $L_1 = 12$mm. (b) $L_1 = 30$mm. (c) $L_1 = 60$mm.

In view of the axial end effect on the three different ironless BLDC motor types, it can be seen from Fig.. 9 that, (i) for

the three motor types used in this part, the axial end effect of the both ends are symmetrical, (ii) the radial magnetic flux density at the axial end of Type III decreases much faster than the other two types, which may be because the magnetic flux density is higher than the other two types, so that more energy is needed to magnetize the air-gap, (iii) the axial end effect cannot be ignored in all the three ironless BLDC motor types, however, it can be ignored in very long machine with thin air-gap length, even if in Fig. 9 (c) good results are obtained.

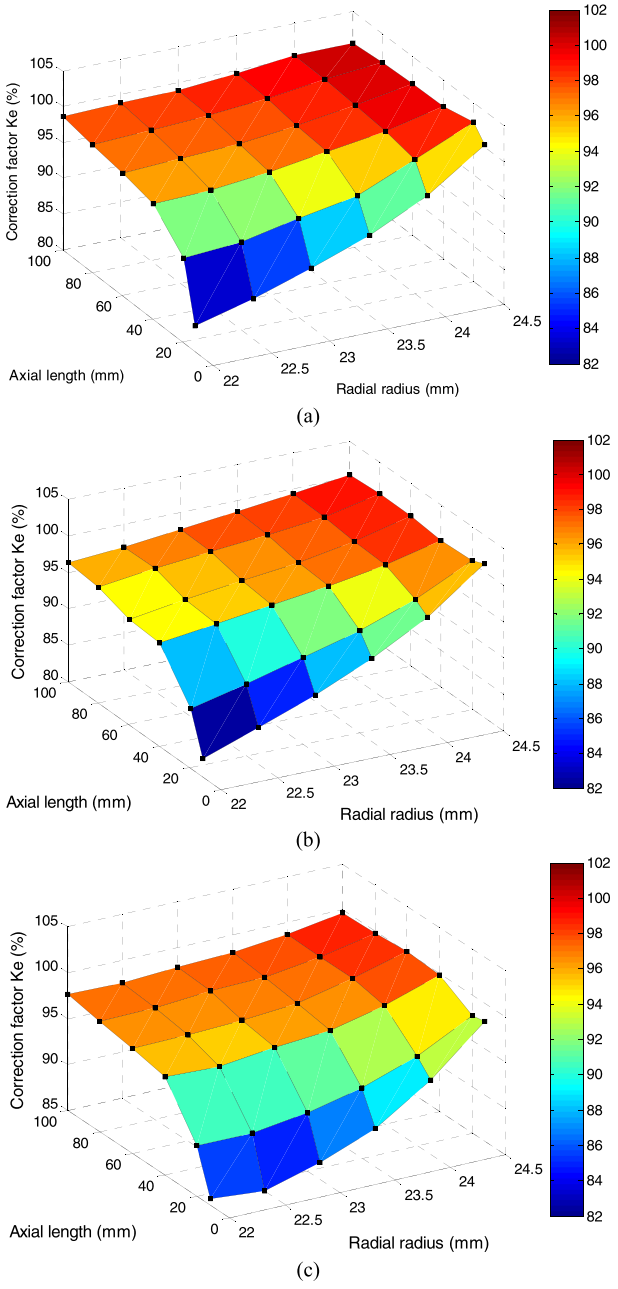

FIGURE 10. Correction factor K_e with different radial radii and axial lengths of the ironless BLDC motor. (a) Type I. (b) Type II. (c) Type III.

Fig. 10 shows the factor K_e for the three different ironless BLDC motor types with cloud diagrams. By adopting the interpolation method, the other K_e values with other axial lengths and radial radii can be obtained. It can be observed from the comprehensive analysis and comparison of Fig. 10 that: (i) for a certain motor of the three investigated ironless BLDC motors in this paper, the correction factor K_e is getting close to 100% with increasing of the axial length and the radial radius, and (ii) the variation range of K_e for Type III is smaller than that of the other two types, which means the axial end effect of Type III is less sensitive to the axial length and radial length.

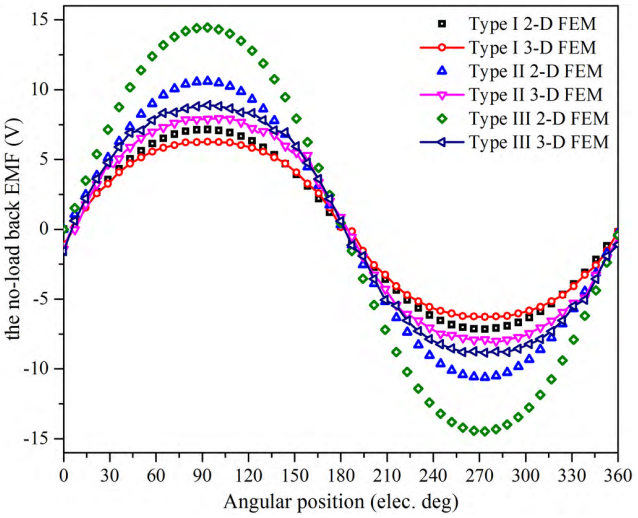

FIGURE 11. The no-load back EMF of 2-D and 3-D FEM of the three different ironless BLDC motor types.

Fig. 11 shows the 2-D and 3-D no-load back EMFs for the three different ironless BLDC motor types using an axial length of 12mm. In this case, the axial end effect was taken into consideration in the 3-D FEM computation. It can be obtained from Fig. 11 that, with the same PMs' magnetization and winding configurations, the 2-D and 3-D FEM results show differences. The back EMFs' amplitude of the three ironless BLDC motors calculated by 2-D FEM at the speed of 6000rpm, are 7.14V, 10.6V and 14.5V, respectively. Correspondingly, the amplitude of the back EMFs calculated by 3-D FEM are 6.28V, 7.9V and 9V. From these differences, it can be inferred that the axial end effect of the presented three ironless BLDC motors should be taken into considerations in the back EMF's calculation.

IV. COMPARISON OF THE TORQUE CHARACTERISTICS

The ironless stator BLDC motors possess zero cogging torque in theory. Besides, the ironless-stator eliminates the stator core loss, and the inner back-irons used in Type II and Type III make the magnetic flux density in Region II bigger than that of in Type I. However, the magnetic field distribution (as it shows in Fig. 9) and back EMF (as it shows in Fig. 11) of the three motor types are much different when considering the axial end effect. The electromagnetic torque and the back EMF are two basic elements in the electromechanical energy

conversion of motors, and considering the law of energy conservation, the output torque is related with the back EMF. Therefore, the torque characteristics of the three ironless BLDC motor types are further studied and compare in this part.

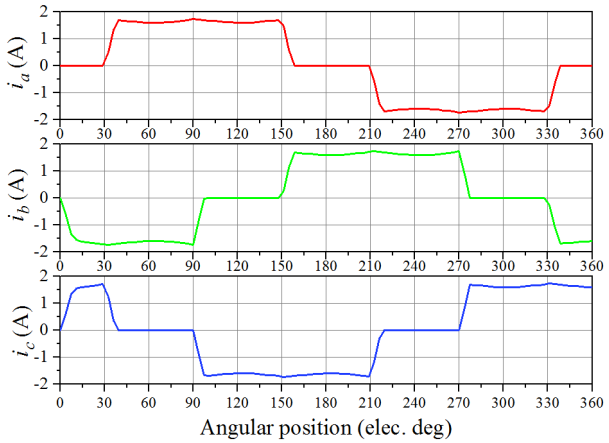

FIGURE 12. The simulated phase current waveforms of ironless BLDC motor of type I at full load and rated speed.

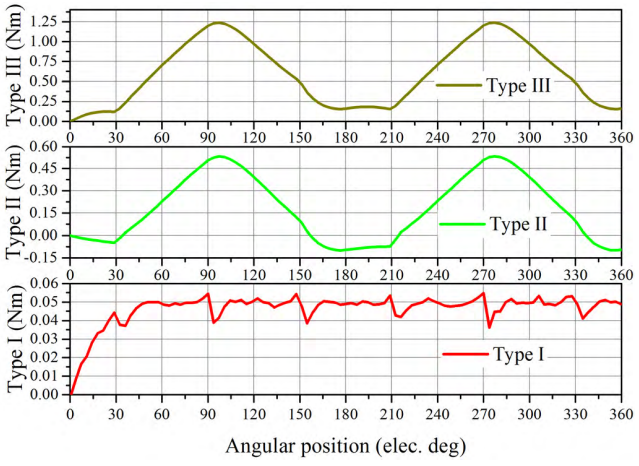

FIGURE 13. The torque with rated input current and speed of the three different ironless BLDC motor types with parallel magnetization.

As is well-known, the electromagnetic torque is generated from the interaction of the phase current and the back EMF. The phase current of the investigated three ironless BLDC motor types is shown in Fig. 12. For BLDC motors' control, the back EMF should be trapezoidal. However, as illustrated in Fig. 11, the back EMF waveforms of the three ironless BLDC motors are sinusoidal, rather than trapezoidal. Fig. 13 shows the torques with rated input current and rated rotational speed of the presented three motor types. It shows that the average torque of Type III is about 3 times bigger than that of type II, owing to extra PMs used on the inner back-iron of the rotor as it shows in Fig. 1 (c), and 17 times bigger than that of Type I. The phase current and non-ideal back EMF will result in critical torque ripple. Besides, the torque

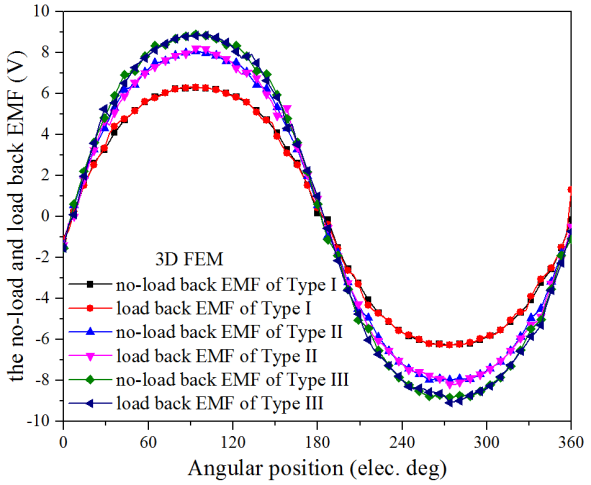

FIGURE 14. The no-load and load back EMF of the presented three different ironless BLDC motors.

ripple of ironless BLDC motors is also related with the phase exchange and the armature reaction. Due to the inductance of the phase windings, the lag of current change during the phase exchange (as illustrated in Fig. 12) will result in torque ripple too. The armature reactions of the presented three ironless BLDC motor types can be reflected by Fig. 14, the little difference between the load and no-load back EMFs may caused by the scale. It shows that the armature reactions are not heavy enough to influence the main magnetic field. Therefore, the serious torque ripples, as shown in Fig. 13, is mainly related to the phase exchange.

V. EXPERIMENT

A prototype of the ironless BLDC motor of Type I with parallel magnetized PMs is manufactured and tested. The stand platform with test and load ironless BLDC motors of Type I is shown in Fig. 15. The stators used for the load and test ironless BLDC motors are made of epoxy resin (a kind of nonmagnetic plastic materials used for motors). The experimental test system is shown in Fig. 16.

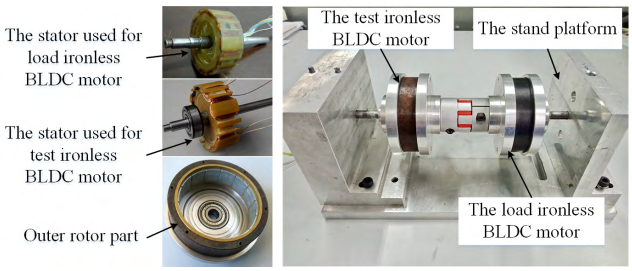

FIGURE 15. The stand platform with test and load ironless BLDC motor of type I.

The no-load back EMF waveform is obtained at the speed of 3800rpm and compared with the FEM computation results, and are shown in Fig. 17. It can be seen that the results obtained from the 2-D FEM computation are higher than

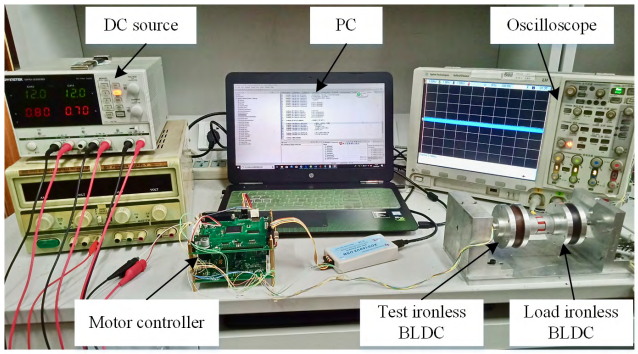

FIGURE 16. Experimental test system.

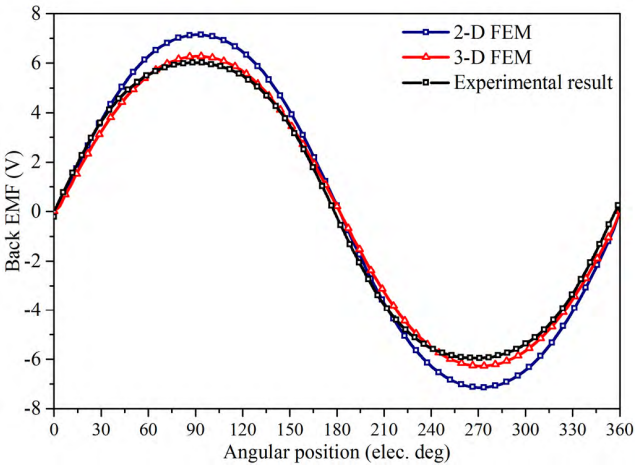

FIGURE 17. The FEM and experimental back EMFs of phase A of Type I.

those from the 3-D FEM computation which accounts for the axial end effect and end windings. The difference between the measured and the calculated by 3-D FEM is about 4%, which thought to be caused by the deficiency of the PMs' magnetic field intensity in real motor topology and the position error of the coils.

VI. CONCLUSION

In this paper, three different ironless BLDC motor types, which are motors without inner back-iron of the rotor (Type I), with inner back-iron of the rotor (Type II) and with dual-rotor (Type III), are investigated. The magnetic characteristics of the three motor types are investigated by FEM. The results show that Type III motor has the largest magnetic load and the most trapezoidal waveform of the radial magnetic flux density. The influence of both the winding configuration and the combination of slot and pole numbers on the back EMF is studied. The evaluation factor ζ_e is proposed to show the influence extent in a quantitative way. The axial end effect of the three motor types are different under the same axial length, and the corresponding correction factor K_e is calculated and compared. As for the torque characteristics, it shows the average torque of Type III is about 3 times bigger than that of type II, and 17 times bigger than that of Type I. Finally, the motor of Type I was manufactured and tested. The results indicate that the axial end effect should not be ignored in the ironless BLDC motors with a short axial length.

REFERENCES

[1] S. J. Park, H. W. Park, M. H. Lee, and F. Harashima, "A new approach for minimum-torque-ripple maximum-efficiency control of BLDC motor," *IEEE Trans. Ind. Electron.*, vol. 47, no. 1, pp. 109–114, Feb. 2000.

[2] H.-W. Lee, T.-H. Kim, and M. Ehsani, "Practical control for improving power density and efficiency of the BLDC generator," *IEEE Trans. Power Electron.*, vol. 20, no. 1, pp. 192–199, Jan. 2005.

[3] K. T. Chau, C. C. Chan, and C. Liu, "Overview of permanent-magnet brushless drives for electric and hybrid electric vehicles," *IEEE Trans. Ind. Electron.*, vol. 55, no. 6, pp. 2246–2257, Jun. 2008.

[4] R. P. Praveen, M. H. Ravichandran, V. T. S. Achari, V. P. J. Raj, G. Madhu, and G. R. Bindu, "A novel slotless Halbach-array permanent-magnet brushless DC motor for spacecraft applications," *IEEE Trans. Ind. Electron.*, vol. 59, no. 9, pp. 3553–3560, Sep. 2012.

[5] Y.-S. Lai and Y.-K. Lin, "A unified approach to zero-crossing point detection of back EMF for brushless DC motor drives without current and Hall sensors," *IEEE Trans. Power Electron.*, vol. 26, no. 6, pp. 1704–1713, Jun. 2011.

[6] X. Chang, Y. Li, W. Zhang, N. Wang, and W. Xue, "Active disturbance rejection control for a flywheel energy storage system," *IEEE Trans. Ind. Electron.*, vol. 62, no. 2, pp. 991–1002, Feb. 2015.

[7] X. Zhou and J. Fang, "Precise braking torque control for attitude control flywheel with small inductance brushless DC motor," *IEEE Trans. Power Electron.*, vol. 28, no. 11, pp. 5380–5390, Nov. 2013.

[8] U. K. Madawala and J. T. Boys, "Magnetic field analysis of an ironless brushless DC machine," *IEEE Trans. Magn.*, vol. 41, no. 8, pp. 2384–2390, Aug. 2005.

[9] R. J. Wang, M. J. Kamper, K. Van der Westhuizen, and J. F. Gieras, "Optimal design of a coreless stator axial flux permanent-magnet generator," *IEEE Trans. Magn.*, vol. 41, no. 1, pp. 55–64, Jan. 2005.

[10] M. Ooshima, S. Kitazawa, A. Chiba, T. Fukao, and D. G. Dorrell, "Design and analyses of a coreless-stator-type bearingless motor/generator for clean energy generation and storage systems," *IEEE Trans. Magn.*, vol. 42, no. 10, pp. 3461–3463, Oct. 2006.

[11] C.-C. Hwang, P.-L. Li, F. C. Chuang, C.-T. Liu, and K.-H. Huang, "Optimization for reduction of torque ripple in an axial flux permanent magnet machine," *IEEE Trans. Magn.*, vol. 45, no. 3, pp. 1760–1763, Mar. 2009.

[12] X. Liu, H. Hu, J. Zhao, A. Belahcen, L. Tang, and L. Yang, "Analytical solution of the magnetic field and EMF calculation in ironless BLDC motor," *IEEE Trans. Magn.*, vol. 52, no. 2, Feb. 2016, Art. no. 8100510.

[13] K. Liu, X. Fu, M. Lin, and L. Tai, "AC copper losses analysis of the ironless brushless DC motor used in a flywheel energy storage system," *IEEE Trans. Appl. Supercond.*, vol. 26, no. 7, pp. 1–5, Oct. 2016.

[14] R. Qu and T. A. Lipo, "Dual-rotor, radial-flux, toroidally wound, permanent-magnet machines," *IEEE Trans. Ind. Appl.*, vol. 39, no. 6, pp. 1665–1673, Nov./Dec. 2003.

[15] M. Galea, L. Papini, H. Zhang, C. Gerada, and T. Hamiti, "Demagnetization analysis for Halbach array configurations in electrical machines," *IEEE Trans. Magn.*, vol. 51, no. 9, Sep. 2015, Art. no. 8107309.

[16] K.-H. Kim, H.-I. Park, S.-M. Jang, and J.-Y. Choi, "Comparison of characteristics of double-sided permanent-magnet synchronous motor/generator according to magnetization patterns for flywheel energy storage system using an analytical method," *IEEE Trans. Magn.*, vol. 51, no. 3, Mar. 2015, Art. no. 8201404.

[17] S. Wu, X. Zhao, Z. Jiao, P. C.-K Luk, and C. Jiu, "Multi-objective optimal design of a toroidally wound radial-flux Halbach permanent magnet array limited angle torque motor," *IEEE Trans. Ind. Electron.*, vol. 64, no. 4, pp. 2962–2971, Apr. 2017.

[18] M. F. J. Kremers, J. J. H. Paulides, J. L. G. Janssen, and E. A. Lomonova, "Design considerations for coreless linear actuators," *IEEE Trans. Magn.*, vol. 49, no. 5, pp. 2271–2274, May 2013.

[19] L. Yan, L. Zhang, Z. Jiao, H. Hu, C.-Y. Chen, and I.-M. Chen, "Armature reaction field and inductance of coreless moving-coil tubular linear machine," *IEEE Trans. Ind. Electron.*, vol. 61, no. 12, pp. 6956–6965, Dec. 2014.

[20] Y. Li, D. Bobba, and B. Sarlioglu, "Design and optimization of a novel dual-rotor hybrid PM machine for traction application," *IEEE Trans. Ind. Electron.*, vol. 65, no. 2, pp. 1762–1771, Feb. 2018.

[21] S. G. Min, D. Bobba, and B. Sarlioglu, "Analysis of overhang effects using conductor separation method in coreless-type PM linear machines," *IEEE Trans. Magn.*, vol. 54, no. 4, Apr. 2018, Art. no. 9300304.
[22] A. Labak and N. C. Kar, "Designing and prototyping a novel five-phase pancake-shaped axial-flux SRM for electric vehicle application through dynamic FEA incorporating flux-tube modeling," *IEEE Trans. Ind. Appl.*, vol. 49, no. 3, pp. 1276–1288, May 2013.
[23] E. Bostanci, Z. Neuschl, R. Plikat, and B. Ponick, "No-load performance analysis of brushless DC machines with axially displaceable rotor," *IEEE Trans. Ind. Electron.*, vol. 61, no. 4, pp. 1692–1699, Apr. 2014.

LIU YANG received the B.E. degree in machine design manufacture and automation from the Inner Mongolia University of Technology, Hohhot, China, in 2012, and the M.Sc. degree in mechanical electronic engineering from Harbin Engineering University, Harbin, China, in 2015. He is currently pursuing the Ph.D. degree with the School of Automation, Beijing Institute of Technology, Beijing, China.

His research interests include the modeling and design of PM machines, and high-precision servo control for positioning systems.

JING ZHAO (M'13) received the B.Sc. degree in electrical engineering from the Hebei University of Technology, Tianjin, China, in 2005, and the M.Sc. and Ph.D. degrees in electrical engineering from the Harbin Institute of Technology, Harbin, China, in 2007 and 2011, respectively.

She is currently an Associate Professor and a Lecturer with the School of Automation, Beijing Institute of Technology, Beijing, China. Her research interests include electric machines and drive systems used for renewable energy and special servo machines systems.

XIANGDONG LIU (M'14) was born in Jingmen, Hubei, China, in 1971. He received the M.S. degree in electrical engineering and the Ph.D. degree in space engineering from the Harbin Institute of Technology, Harbin, China, in 1995 and 1998, respectively.

He is currently a Professor with the School of Automation, Beijing Institute of Technology, Beijing, China. His research interests include high-precision servo control, motor drive control, piezoceramics actuator drive and compensation control, sliding control, state estimation, and attitude control.

A. HADDAD (M'13) received the bachelor's degree in electrical engineering in 1985 and the Ph.D. degree in high voltage engineering in 1990. He is currently a Professor with Cardiff University. He has published an IET-power series book *Advances in High Voltage Engineering*. His research interests are in overvoltage protection, insulation systems, insulation coordination, and earthing systems. He is a member of CIGRE working groups and BSI PEL1/2, IEC TC37.

He is a fellow of the IET and the Learned Society of Wales. He serves on the scientific committees of several international conferences.

JUN LIANG (M'02–SM'12) received the B.Sc. degree from the Huazhong University of Science and Technology, Wuhan, China, in 1992, and the M.Sc. and Ph.D. degrees from the China Electric Power Research Institute, Beijing, China, in 1995 and 1998, respectively. From 1998 to 2001, he was a Senior Engineer with the China Electric Power Research Institute. From 2001 to 2005, he was a Research Associate with Imperial College London, London, U.K. From 2005 to 2007, he was a Senior Lecturer with the University of Glamorgan, Wales, U.K. He is currently a Professor with the School of Engineering, Cardiff University, Wales. His research interests include power system stability and control, power electronics, and renewable power generation.

HENGZAI HU received the B.E. degree in automation from the Hebei University of Technology, Tianjin, China, and the Ph.D. degree from the Beijing Institute of Technology, Beijing, China, in 2011 and 2017, respectively.

He is currently an Electrical Engineer with the Beijing Machine and Equipment Institute, Beijing. His research interests include the modeling and design of linear PM machines and high-precision servo control for positioning systems.